Cell Metabolism
Short Article

Diet-Induced Unresolved ER Stress Hinders KRAS-Driven Lung Tumorigenesis

Giorgio Ramadori,[1,6] Georgia Konstantinidou,[2,6,7] Niranjan Venkateswaran,[2] Tommasina Biscotti,[3] Lorraine Morlock,[4] Mirco Galié,[1] Noelle S. Williams,[4] Michele Luchetti,[5] Alfredo Santinelli,[3] Pier Paolo Scaglioni,[2,*] and Roberto Coppari[1,*]
[1]Department of Cell Physiology and Metabolism, University of Geneva, 1211 Geneva 4, Switzerland
[2]Department of Internal Medicine, Simmons Cancer Center, University of Texas Southwestern Medical Center, Dallas, TX 75390, USA
[3]Section of Pathological Anatomy, Department of Biomedical Sciences and Public Health, Università Politecnica delle Marche, 60020 Ancona, Italy
[4]Department of Biochemistry, University of Texas Southwestern Medical Center, Dallas, TX 75390, USA
[5]Clinica Medica, Dipartimento di Scienze Cliniche e Molecolari, Università Politecnica delle Marche, 60020 Ancona, Italy
[6]Co-first author
[7]Present address: Department of Molecular Biology, University of Geneva, 1211 Geneva 4, Switzerland
*Correspondence: pier.scaglioni@utsouthwestern.edu (P.P.S.), roberto.coppari@unige.ch (R.C.)
http://dx.doi.org/10.1016/j.cmet.2014.11.020

SUMMARY

Dietary effects on tumor biology can be exploited to unravel cancer vulnerabilities. Here, we present surprising evidence for anti-proliferative action of high-calorie-diet (HCD) feeding on KRAS-driven lung tumors. Tumors of mice that commenced HCD feeding before tumor onset displayed defective unfolded protein response (UPR) and unresolved endoplasmic reticulum (ER) stress. Unresolved ER stress and reduced proliferation are reversed by chemical chaperone treatment. Whole-genome transcriptional analyses revealed FKBP10 as one of the most downregulated chaperones in tumors of the HCD-pre-tumor-onset group. FKBP10 downregulation dampens tumor growth in vitro and in vivo. Providing translational value to these results, we report that FKBP10 is expressed in human KRAS-positive and -negative lung cancers, but not in healthy parenchyma. Collectively, our data shed light on an unexpected anti-tumor action of HCD imposed before tumor onset and identify FKBP10 as a putative therapeutic target to selectively hinder lung cancer.

INTRODUCTION

Feeding on a high-calorie diet (HCD) causes obesity and diabetes (Vianna and Coppari, 2011), which are known cancer risk factors (Bianchini et al., 2002; Calle and Kaaks, 2004; Calle and Thun, 2004; Khandekar et al., 2011). Thus, gaining a better understanding of the relationship between increased calorie intake and cancer is urgent, as it will provide insights into the mechanisms of cancer pathogenesis.

Increased anabolic signaling caused by HCD may explain higher cancer risk in obesity (Taubes, 2012). For example, HCD increases blood levels of anabolic citokines (e.g., insulin, insulin-like growth factors, and leptin) that are known to promote tumor growth and survival by signaling via the PI3K-AKT-mTOR and RAS-MAPK pathways (Banks et al., 2000; Engelman, 2009; Schubbert et al., 2007; Vansaun, 2013; Zoncu et al., 2011). Another well-established event associated with HCD is the increased inflammatory (e.g., TNF-α) signaling, which is also known to favor tumorigenesis (Park et al., 2010a).

Lung cancer is the leading cause of cancer-related death worldwide, with non-small cell lung cancer (NSCLC) representing almost 85% of all cases. Activating mutations of the proto-oncogene *KRAS* (mutant *KRAS*) occur in ~30% of NSCLC cases (Pylayeva-Gupta et al., 2011). Mutant KRAS-driven tumors are associated with an aggressive phenotype, resistance to therapy, and poor outcome (Pao et al., 2005). The results from epidemiological studies assessing the effect of obesity on lung cancer risk are still inconclusive (Calle and Kaaks, 2004; Dahlberg et al., 2013; Leung et al., 2011; Yang et al., 2013).Yet, calorie restriction exerts a robust anti-tumor effect on KRAS-driven lung cancer in rodents (Kalaany and Sabatini, 2009), indicating that this type of tumor is sensitive to dietary changes. However, preclinical studies assessing KRAS-driven lung tumorigenesis in the context of increased calorie intake are missing. We reasoned that if HCD feeding interferes with KRAS-driven lung tumorigenesis, then the study of this contextual effect could be exploited to unmask key cancer vulnerabilities. Hence, we assessed the impact of HCD feeding on KRAS-driven lung tumors in mice.

RESULTS

A Dual Effect of Chronic HCD Feeding on KRAS-Driven Lung Tumorigenesis

To comprehensively analyze the effect of HCD feeding on lung tumors in vivo, we fed genetically modified mice that develop KRAS-driven lung tumors (i.e., $Kras^{G12D}$ mice) with HCD starting before or after tumor onset. $Kras^{G12D}$ mice were obtained by breeding a transgene encoding $Kras^{G12D}$ under the control of the tetracycline operator (*Tet-op-Kras*) to a transgene expressing the reverse tetracycline transactivator in the respiratory epithelium under the control of the Clara cell secretory protein promoter (*CCSP-rtTA*). The resulting bi-transgenic $Kras^{G12D}$

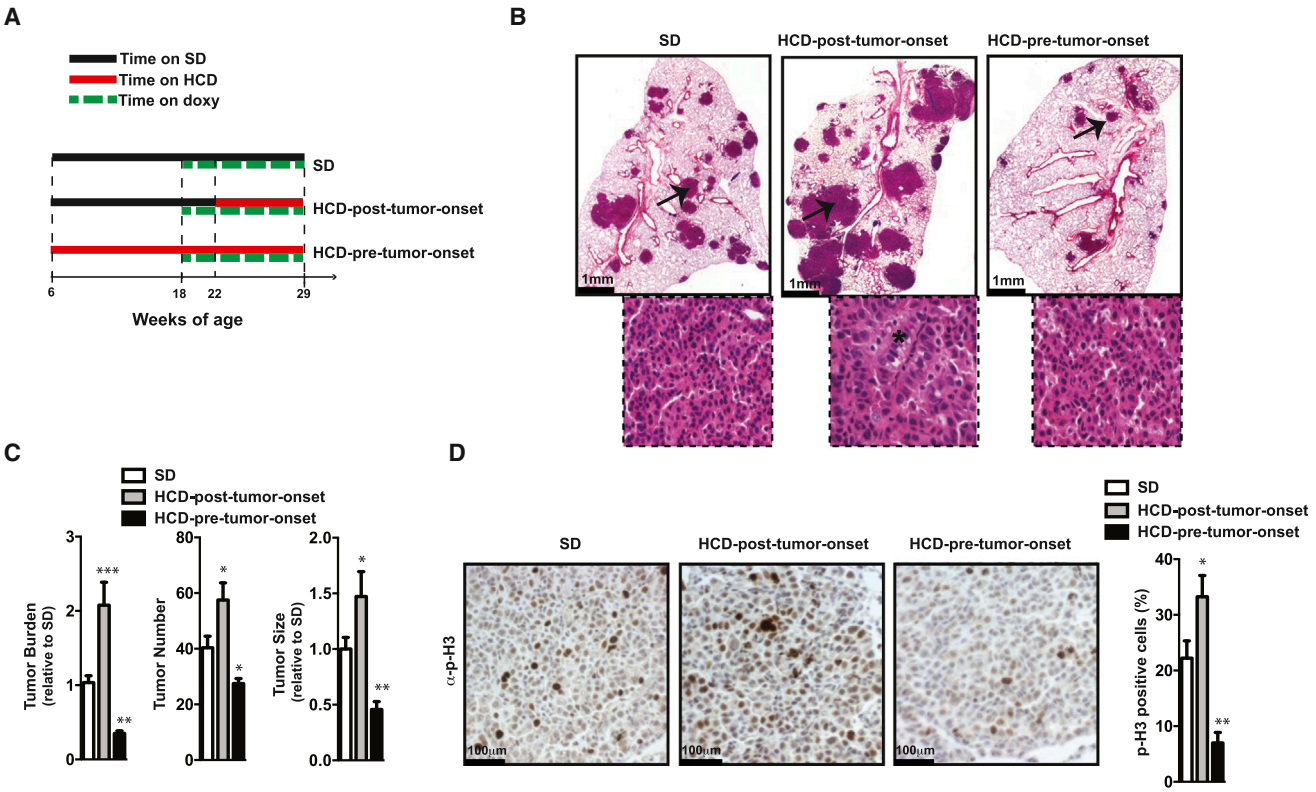

Figure 1. A Dual Effect of Chronic HCD Feeding on KRAS-Driven Lung Tumorigenesis

(A) Timetable of mouse treatments.

(B) Representative images of lung sections stained with hematoxylin and eosin (H&E) (inserts indicate area selected by arrows for higher magnification images; asterisk indicates the presence of nests of cells with large atypical nuclei).

(C) Histograms showing quantification of tumor burden, size, and number.

(D) Representative images of lung sections stained with anti-p-H3 (p-H3-positive cells in dark brown) and histograms indicating the percentage of p-H3-positive cells/tumor cells.

Data shown in (B)–(D) are from 29-week-old $Kras^{G12D}$ mice treated as in (A) (females, n = 6–7/ group). Error bars represent SEM. Statistical analyses were done using one-way ANOVA (Tukey's post test). *p < 0.05, **p < 0.01, ***p < 0.001. See also Figure S1.

mice develop lung cancer with 100% penetrance following continuous doxycycline (doxy) administration (Fisher et al., 2001). The effect of the different dietary treatments on lung tumors was assessed by comparing neoplastic lesion profiles between three groups: (i) $Kras^{G12D}$ mice constantly fed a standard diet (SD $Kras^{G12D}$ group), (ii) $Kras^{G12D}$ mice switched and maintained on a HCD starting 4 weeks after tumor induction (HCD-post-tumor-onset $Kras^{G12D}$ group), and (iii) $Kras^{G12D}$ mice switched and maintained on a HCD starting 12 weeks before tumor induction (HCD-pre-tumor-onset $Kras^{G12D}$ group) (Figure 1A). In all groups tumorigenesis was induced at the age of 18 weeks by doxy treatment, and endpoint analyses were performed at the age of 29 weeks (Figure 1A).

HCD-pre-tumor-onset $Kras^{G12D}$ mice (18 and 29 weeks old) had increased body weight, hyperinsulinemia, and hyperleptinemia, while these parameters were all normal in HCD-post-tumor-onset $Kras^{G12D}$ mice compared to age-matched SD $Kras^{G12D}$ mice. However, at the age of 29 weeks both HCD-fed groups displayed increased hepatic lipid accumulation (Figures S1A–S1C, available online).

Strikingly, endpoint analysis of the lungs revealed opposite effects of the two different HCD feeding regimens on neoplastic lesions. The HCD-post-tumor-onset $Kras^{G12D}$ mice had a significant increase in tumor burden owing to increased tumor size and number, while HCD-pre-tumor-onset $Kras^{G12D}$ mice had these parameters significantly reduced compared to those of SD $Kras^{G12D}$ mice (Figures 1B and 1C). Notably, the tumor burden-, size-, and number-suppressing effect of pretreatment with HCD applied to both genders (Figures 1B, 1C, and S1D).

Histopathological examination indicated that neoplastic lesions from all groups were adenomas (Figure 1B).Yet, lesions from HCD-post-tumor-onset $Kras^{G12D}$ mice were distinguished by the presence of nests of cells containing large atypical nuclei (Figure 1B), indicating a more advanced tumor grade.

Next, we set out to determine the underlying mechanism of HCD effect on tumor growth. As the tumor formation and maintenance in $Kras^{G12D}$ mice is strictly dependent on oncogenic $Kras^{G12D}$ expression (Fisher et al., 2001), we measured $Kras^{G12D}$ mRNA level in tumor lesions. This parameter was similar between groups (Figure S1E), hence ruling out the idea that the different tumor growth observed between groups was the consequence of dietary effects on $Kras^{G12D}$ expression.

Changes in tumor growth could be the result of altered cellular death, altered cellular proliferation, or both. Notably,

while the status of apoptosis markers (assessed by TUNEL assay and immunostaining for cleaved caspase-3) was unchanged (Figures S1F and S1G), the expression levels of proliferation markers (p-H3 and cyclin-D1) were significantly reduced in tumors of HCD-pre-tumor-onset compared to SD *Kras*^{G12D} mice (Figures 1D and S1H). Conversely, cellular proliferation was increased in HCD-post-tumor-onset compared to SD *Kras*^{G12D} mice (Figure 1D). HCD feeding could also impact tumor initiation. For instance, inflammation caused by dietary obesity is an effective tumor promoter in a model of hepatocellular carcinoma (Park et al., 2010a). In addition, recent studies have shown that chronic pancreatitis is required for KRAS-induced pancreatic ductal adenocarcinomas in adult mice (Guerra et al., 2007). Therefore, nongenetic events associated with HCD feeding could modulate tumor initiation when the latter is driven by a defined oncogenic mutation including *KRAS* (Guerra et al., 2007; Park et al., 2010a). Notably, lungs of SD or HCD-pre-tumor-onset *Kras*^{G12D} mice treated with doxy for 4 weeks had no differences in tumor size and multiplicity (Figure S1I). Combined, these findings indicate that HCD feeding imposed before tumor onset affects tumor progression rather than initiation.

Collectively, our results show that HCD feeding started before or after tumor onset can inhibit or promote KRAS-driven lung tumorigenesis by mechanisms that involve suppression or enhancement of cellular proliferation, respectively.

Chronic HCD Feeding Causes Unresolved ER Stress in KRAS-Driven Lung Tumors

We uncovered a surprising and potent anti-tumor effect of HCD imposed before tumor onset. This finding prompted us to look for the underlying mechanism because it could unveil key vulnerabilities of KRAS-driven lung tumors. To this end, we first analyzed the activation status of anabolic signaling pathways known to promote tumorigenesis and be altered in the context of increased calorie intake (i.e., AKT, ERK, and STAT3) (Banks et al., 2000; Engelman, 2009; Schubbert et al., 2007; Taubes, 2012; Vansaun, 2013; Zoncu et al., 2011). For instance, chronic HCD feeding induces systemic insulin resistance characterized by reduced insulin/AKT signaling in metabolically relevant tissues (Ramadori et al., 2011). Thus, reduced AKT signaling in tumors from HCD-pre-tumor-onset *Kras*^{G12D} mice could in principle explain the reduced neoplastic growth. However, while we found reduced insulin-induced phosphorylation of AKT, the basal level of phosphorylated AKT and of one of its downstream targets ribosomal protein S6 was similar between tumors of HCD-pre-tumor-onset and SD *Kras*^{G12D} mice (Figures S2A and S2B). These data suggest that exacerbated insulin resistance in tumors of HCD-pre-tumor-onset *Kras*^{G12D} mice is not sufficient to dampen basal AKT signaling. Also, the status of phosphorylation and thus activation of ERK and STAT3 signaling was unchanged in HCD-pre-tumor-onset compared to SD *Kras*^{G12D} mice (Figure S2B).

An expected consequence of chronic HCD feeding is increased inflammatory signaling. Indeed, we found that the serum level of the proinflammatory cytokine interleukin-6 (IL-6) and the mRNA level of intracellular inflammatory readouts (e.g., *Ik-Bα* and *Tnf-α*) were elevated in tumors of HCD-pre-tumor-onset compared to SD *Kras*^{G12D} mice (Figures S2C–S2E). Collectively, the aforementioned results suggest that changes in basal AKT, ERK, STAT3, or inflammatory signaling are likely not underlying the antiproliferative effects of nutritional overload on KRAS-driven lung tumors.

Next, we assessed whole-genome expression profile of microdissected lung tumors and found a significantly reduced expression of chaperones in lung tumors of HCD-pre-tumor-onset compared to SD *Kras*^{G12D} mice (Figures 2A and S2F). Several of these chaperones are established or predicted ER residents. ER chaperones are essential for normal protein folding and key components of the ER-induced UPR (UPR^{ER}), a cellular mechanism limiting the degree of ER stress due to the accumulation of unfolded proteins in the ER (Walter and Ron, 2011). Thus, we hypothesized that tumor cells in HCD-pre-tumor-onset *Kras*^{G12D} mice may be unable to mount an effective UPR^{ER}. To directly address this idea, we further characterized the status of the UPR^{ER} in tumors of these mice. X-box binding protein 1 (XBP1) is an essential component of the UPR, and in response to ER stress it is spliced to produce the nuclear-localized active transcription factor XBP1s (Walter and Ron, 2011). Similarly, chronic HCD feeding induced *Xbp1* mRNA splicing in lung tumor tissue of HCD-pre-tumor-onset *Kras*^{G12D}, as indicated by increased and decreased *Xbp1s* and *Xbp1*-unspliced (*Xbp1-u*) mRNAs, respectively (Figure 2B). However, despite the increased amount of cytosolic XBP1s, the amount of nuclear XBP1s was lower in lung tumors of HCD-pre-tumor-onset compared to SD *Kras*^{G12D} mice (Figure 2C). This result is in line with the reduced mRNA level of the ER chaperones *Erdj4*, *p58ipk*, *Pdia3*, and *Hedj* (which are known transcriptional targets of XBP1s) in tumors of HCD-pre-tumor-onset compared to SD-fed *Kras*^{G12D} mice (Figure 2D). Consistently, protein content of the same chaperones was also reduced (Figure 2E). Collectively, these results indicate a defective UPR^{ER} in tumors of HCD-pre-tumor-onset mice.

To independently assay ER stress level, we measured the status of several ER stress transducers. Our data show that the phosphorylation level of eukaryotic translational initiation factor 2α (eIF2α), of ER transmembrane kinase/endoribonuclease (RNase) IRE1α, and activation of c-Jun N-terminal kinase (JNK), all of which are found to be increased upon ER stress (Ozcan et al., 2004; Ozcan et al., 2006), were significantly higher in tumors of HCD-pre-tumor-onset compared to SD-fed *Kras*^{G12D} mice (Figure 2F). Notably, increased p-eIF2α is expected to lead to cell-cycle attenuation or even arrest in proliferating cells (Ranganathan et al., 2008; Ron, 2002), a result consistent with reduced tumor proliferation in HCD-pre-tumor-onset *Kras*^{G12D} mice (Figures 1D and S1H).

Interestingly, mRNA level of another component of the UPR^{ER}, and a major component of the ER stress-mediated apoptosis pathway, C/EBP homologous protein (CHOP) was downregulated in tumors of HCD-pre-tumor-onset compared to SD *Kras*^{G12D} mice (Figure 2G). These data are consistent with reduced expression of death receptor-5 (*Dr5*) (Figure S2G), a transcriptional target of CHOP and an important mediator of ER-stress-mediated apoptosis (Lu et al., 2014). CHOP regulates ER-stress-induced apoptosis also by repressing *Bcl2* gene expression (Szegezdi et al., 2006) whose expression was similar in tumors of the different dietary groups (Figure S2G), another result that does not support CHOP-induced activation of apoptotic signaling. We suggest that reduced *Chop* expression

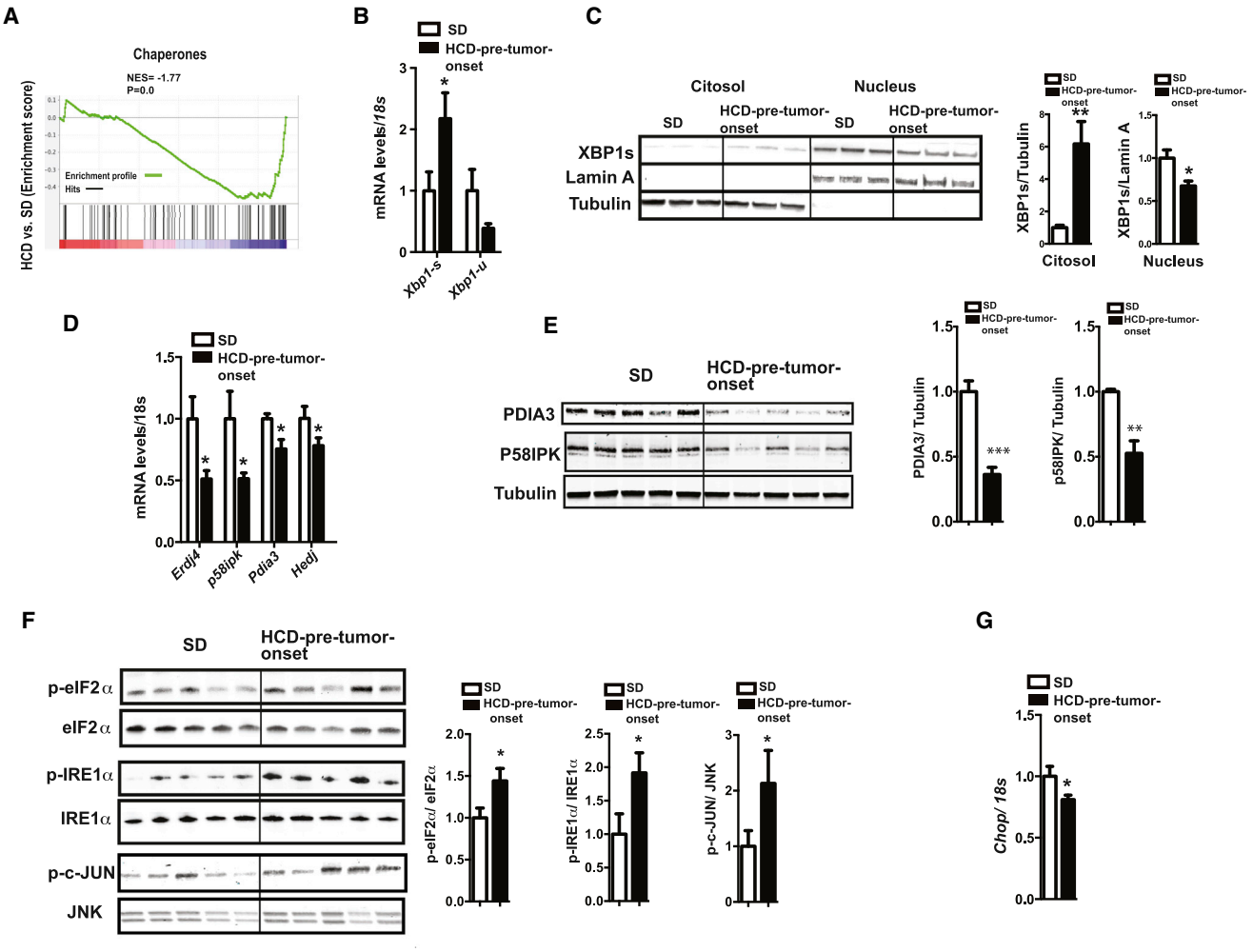

Figure 2. Unresolved ER Stress in Lung Tumors of HCD-Pre-Tumor-Onset *Kras*^{G12D} Mice

(A) Gene set enrichment analysis (GSEA) plot showing chaperone enrichment score depicted by NES and nominal p value (the gene set used for GSEA is GO: 0006457).

(B) *Xbp1s* and *Xbp1u* mRNA levels.

(C) Immunoblot images and quantifications of cytosolic and nuclear XBP1 protein content (Lamin A and Tubulin were used as nuclear and cytosolic markers, respectively).

(D) mRNA levels of ER chaperones.

(E) Immunoblot images and quantification of ER chaperone protein content in total cell lysate.

(F) Immunoblot images and quantification of the phosphorylation status of eIF2α, IRE1α, and c-JUN.

(G) *Chop* mRNA levels.

All panels show data from microdissected lung tumors of 29-week-old *Kras*^{G12D} males treated as described in Figure 1A (n = 5–6/group). Error bars represent SEM. Statistical analyses were done using two-tailed unpaired Student's t test. *p < 0.05, **p < 0.01, ***p < 0.001. See also Figure S2.

may explain, at least in part, why unresolved ER stress does not lead to apoptosis in tumors of HCD-pre-tumor-onset *Kras*^{G12D} mice.

Healthy lung tissue (tumor free) from HCD-pre-tumor-onset *Kras*^{G12D} mice had increased ER stress compared to SD controls, as determined by *Xbp1s*, p-eIF2α, and p-IRE1α level (Figures S2H and S2I). However, the increased nuclear accumulation of XBP1s and the increased expression of ER chaperones and *Chop* (Figures S2J–S2L) indicated normal UPR^{ER} activation in this tissue. Notably, the levels of the aforementioned ER stress and UPR^{ER} activation markers and XBP1s protein contents were not different between tumors from HCD-post-tumor-onset and SD *Kras*^{G12D} mice (Figures S2M–S2Q). Altogether, our data indicate a tumor-specific defect in ER chaperone expression in lungs of *Kras*^{G12D} mice that strongly depends on the time HCD feeding is initiated relative to tumor onset.

Chaperones are also essential for the mitochondrial-induced UPR (UPR^{mt}), a response aimed at maintaining proper protein folding in the mitochondrial matrix (Pellegrino et al., 2013). UPR^{mt} is activated when mitochondrial protein balance is disrupted and is associated with mitochondrial and nuclear gene expression imbalance (Mouchiroud et al., 2013; Pellegrino et al., 2013). Our data show reduced expression of mitochondrial matrix chaperones in tumors of HCD-pre-tumor-onset *Kras*^{G12D} mice

compared to their lean controls (Figure S2R). However, no changes in the ratio between nuclear DNA-encoded *Atp5a1* and mitochondrial DNA-encoded *Mtco1* (Figure S2S) were observed. Moreover, level of protein carbonylation and expression of detoxification enzymes catalase (*Cat*) and superoxide dismutase 2 (*Sod2*) did not differ between tumors from different dietary groups (Figures S2T and S2U), indicating a similar level of reactive oxygen species. These results suggest that reduced expression of mitochondrial chaperones in tumors of HCD-pre-tumor-onset compared to SD $Kras^{G12D}$ mice did not cause significant changes in UPR^{mt} and mitochondrial function; hence, it is not likely to be the reason for the anti-tumor effect of HCD feeding.

Collectively, our data indicate that HCD feeding started before tumor onset causes impaired UPR^{ER} response and consequentially unresolved ER stress in KRAS-driven lung tumors.

Treatment with Chemical Chaperones Reverses the Anti-Tumor Effect of HCD Feeding on KRAS-Driven Lung Tumors

Our results prompted us to directly test whether the anti-tumor action of HCD on KRAS-driven lung tumors is the result of unresolved ER stress. If unresolved ER stress underlies the antiproliferative effect of HCD feeding, its rescue in HCD-pre-tumor-onset $Kras^{G12D}$ mice should boost tumor growth to a level similar to that of SD $Kras^{G12D}$ mice. Administration of chemical chaperones, such as taurorsodeoxycholic acid (TUDCA) or 4-phenyl butyric acid (4-PBA), resolves ER stress induced by increased calorie intake (Ozcan et al., 2006). Thus, we tested whether treatment with TUDCA or 4-PBA reverses the anti-tumor action of HCD on Kras-driven lung tumors.

During the last 2 weeks of doxy treatment, HCD-pre-tumor-onset $Kras^{G12D}$ mice were additionally treated daily with TUDCA (or saline) (Figure 3A). While tumor burden was again significantly reduced in saline-injected HCD-pre-tumor-onset compared to SD $Kras^{G12D}$ mice, it was comparable between these groups following TUDCA administration (Figures 3B and 3C). The increased tumor burden in TUDCA-injected HCD-pre-tumor-onset $Kras^{G12D}$ mice was the result of increased tumor size, but not tumor number (Figure 3C). Tumor burden, number, and size were not affected by TUDCA administration in SD $Kras^{G12D}$ mice (Figures 3B and 3C). Pharmacokinetic assessments revealed a similar level of TUDCA accumulation in lung tumors between the different dietary groups (Figures S3A and S3B). Moreover, the treatment of HCD-pre-tumor-onset $Kras^{G12D}$ mice with TUDCA resulted in attenuation of ER stress to a level similar to that of SD $Kras^{G12D}$ mice, as evidenced by expression of ER stress markers (Figures 3D, 3E, and S3C). These effects were not secondary to changes in body weight, insulinemia, and leptinemia, as these parameters were not different between TUDCA-treated and saline-treated HCD-pre-tumor-onset $Kras^{G12D}$ mice (data not shown). In line with the fact that chronic HCD feeding caused reduced cellular proliferation (Figures 1D and S1H), TUDCA reversed the antiproliferative effect of chronic HCD pretreatment on KRAS-driven lung tumors, as indicated by increased expression of p-H3 (Figure 3F). Notably, the tumor-proliferating effect of TUDCA was not associated with changes in mitochondrial:nuclear gene expression ratio (Figure S3D) or in protein carbonylation level (Figure S3E).

Similar treatment with another structurally unrelated chemical chaperone 4-PBA (Figure S3F) essentially reproduced the effect of TUDCA by relieving ER stress and partially rescuing proliferation and growth of tumors of HCD-pre-tumor-onset $Kras^{G12D}$ mice (Figures S3G–S3I and data not shown).

Altogether, our data indicate that chronic HCD feeding impairs UPR^{ER} and consequently causes unresolved ER stress that hinders the growth of $Kras^{G12D}$-driven lung tumors.

Unraveling FKBP10 as a Target for KRAS-Driven Lung Cancer

Our data suggest that the inhibition of ER chaperones whose expression is negatively affected by HCD pretreatment may represent an effective antiproliferative therapeutic avenue against KRAS-driven lung cancer. A major drawback of current treatments against KRAS-driven lung cancer is the toxic side effects of the drugs due to the lack of selectivity between cancer and normal cells. Therefore, we reasoned that an ideal target against KRAS-driven lung cancer could be an ER chaperone expressed in tumor lesions but not healthy parenchyma.

In order to determine a candidate target, we analyzed our microarray data searching for chaperones that are (i) a resident of the ER, (ii) significantly downregulated in tumors of HCD-pre-tumor-onset $Kras^{G12D}$ mice compared to SD controls, and (iii) specifically expressed in tumor lesions. We found several ER chaperones downregulated in tumors of HCD-pre-tumor-onset $Kras^{G12D}$ mice (Figure S2F). One of them, namely FKBP10, has been reported not to be expressed in lung during adulthood (Lietman et al., 2014; Patterson et al., 2000). Our data indicate that FKBP10 is (i) expressed in tumors of $Kras^{G12D}$ mice, (ii) reduced in tumors of HCD-pre-tumor-onset mice compared to their SD controls, and (iii) barely detectable in normal lung parenchyma (Figure 4A). Therefore, FKBP10 could be an ideal cancer-selective target against Kras-driven lung tumorigenesis. To our knowledge, the role of FKBP10 in tumorigenesis is unknown.

Next, we assessed the significance of FKBP10 in human lung cancer cell lines and found that it is required for proliferation of lines bearing *KRAS* mutation or mutations different from *KRAS* (i.e., *EGFR* or *PI3K* oncogenic mutations) (Figures 4B and 4C). Our in vivo data also show that knockdown of FKBP10 is sufficient to hinder tumor growth (Figure 4D). This anti-tumor effect is caused by reduced cellular proliferation, as determined by reduced cyclin-D1 and p-H3 (Figures 4E and S4A), and not an increased rate of apoptosis (Figure S4B). Notably, our data indicate that the antiproliferative effect of FKBP10 knockdown is not restricted to lung cancer cell lines but extends to cancer cells derived from other tissues (i.e., breast and pancreas) (Figures S4C and S4D).

To add translational value to our preclinical studies, we assessed expression of FKBP10 in surgically collected human lung samples containing tumor lesions and healthy parenchyma. Importantly, our results indicate that FKBP10 is expressed in KRAS-positive and -negative lung carcinoma, but not in healthy lung parenchyma (Figures 4F and 4G). Collectively, our data suggest that inhibition of FKBP10 is a promising avenue to selectively hinder lung cancer growth while sparing healthy lung tissue function.

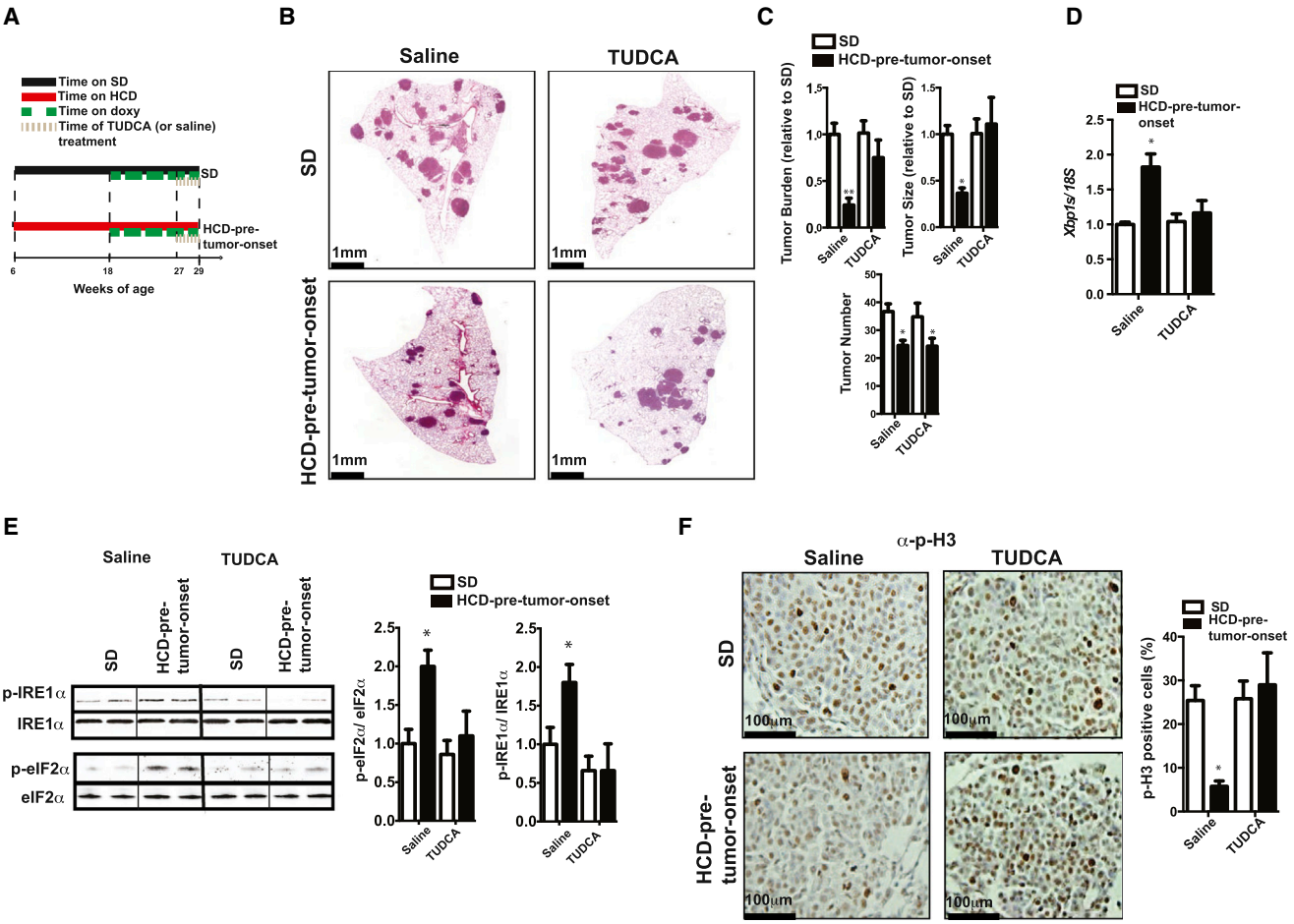

Figure 3. TUDCA Treatment Reverses the Anti-Tumor Effect of HCD Feeding on KRAS-Driven Lung Tumors

(A) Timetable of mouse treatments.

(B) Representative images of lung sections stained with H&E.

(C) Histograms indicating quantification of tumor burden, size, and number.

(D) mRNA levels of *Xbp1s*.

(E) Representative immunoblot against phospho- and total IRE1α and eIF2α.

(F) Representative images of lung sections stained with anti-p-H3 (p-H3-positive cells in brown) and histograms indicating the percentage of p-H3-positive cells/tumor cells of microdissected tumors.

Data shown in (B)–(F) are from 29-week-old $Kras^{G12D}$ mice treated as indicated in (A) (females, n = 5/group). Error bars represent SEM. Statistical analyses were done using one-way ANOVA (Tukey's post test). *p < 0.05, **p < 0.01. See also Figure S3.

DISCUSSION

Our data challenge the common wisdom that HCD feeding exerts only deleterious effects. In fact, we demonstrate that if HCD starts before tumor onset it dampens growth of KRAS-driven lung tumors (Figures 1A–1C). However, an opposite outcome is caused by HCD starting after tumor onset (Figures 1A–1C). Hence, the anti-tumor effect is not due to the diet per se but depends on when HCD feeding is initiated relative to tumor onset.

Our results indicate that impaired UPR^{ER} underlies, at least in part, the anti-tumor action of HCD imposed before tumor onset. We suggest that a contributor to impaired UPR^{ER} is the poor cytosol-to-nucleus translocation of XBP1s, a defect consistent with insulin resistance in tumors of HCD-pre-tumor-onset compared to SD $Kras^{G12D}$ mice (Figure S2A) (Lee et al., 2011; Park et al., 2010b, 2014). Additional studies are needed to test this possibility.

Why does HCD feeding imposed before tumor onset hinder tumor progression but not tumor initiation (Figures 1B, 1C, and S1I)? We propose that this could be explained, at least in part, by an effect of the HCD on tumor vascularization, as CD31-positive cells were found to be diminished in tumors of HCD-pre-tumor-onset mice compared to the SD $Kras^{G12D}$ mice (G.R., G.K., and R.C. unpublished data). In fact, this difference may not lead to relevant effects at the initial stage of the tumorigenesis (when tumor lesions are sufficiently vascularized by the vessels in the parenchyma) but may become a limiting factor for further tumor progression, a hypothesis that warrants future experimental testing.

The clinical relevance of our results is at least 2-fold. First, our data suggest that inhibition of chaperones downregulated by

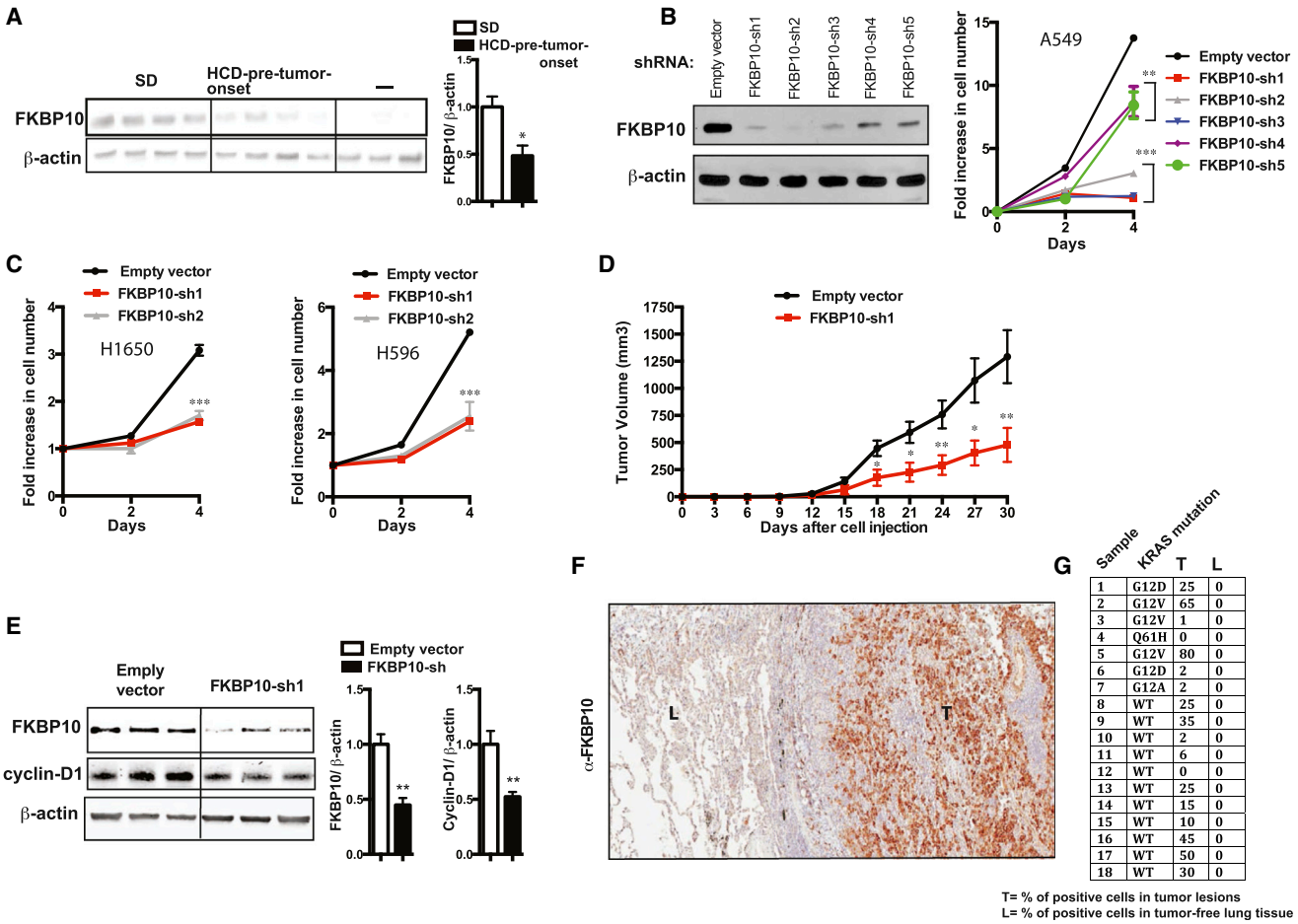

Figure 4. Unraveling FKBP10 as a Therapeutic Target for KRAS-Driven Lung Cancer

(A) Expression of FKBP10 in lung tumors of 29-week-old *Kras*^{G12D} mice treated as in Figure 1A (males, n = 5–6/group) (as negative control [–], we loaded a similar amount of lysate from wild-type lung tissue).

(B) Knockdown in A549 cells (*KRAS* mutation) of FKBP10 using five different shRNAs and relative proliferation curves.

(C) Antiproliferative effect of FKBP10 knockdown in H1650 (*EGFR* mutation) and A596 (*PI3K* mutation) cell lines.

(D) Xenograft growth of A549 cells in SCID mice injected subcutaneously with 1 × 10^6 cells as indicated (n = 5 for group).

(E) Immunoblot from tumors of mice treated as indicated in (D).

(F) Representative images of a human lung section stained against FKBP10 ("L" indicates tumor-free lung parenchyma; "T" indicates lung tumor lesion).

(G) Table indicating the expression of FKBP10 in human specimens including tumor lesions and adjacent tumor-free tissue. Error bars represent SEM. Statistical analyses were done using two-tailed unpaired Student's t test or using one-way ANOVA (Tukey's post test). *p < 0.05, **p < 0.01, ***p < 0.001. See also Figure S4.

HCD pretreatment (e.g., FKBP10) may reduce KRAS-driven lung tumor growth. Second, our data suggest that TUDCA or PBA treatment improves ER stress, therefore leading to increased growth of already-formed KRAS-driven lung tumors in the context of obesity. Because TUDCA and PBA are currently undergoing evaluation (http://clinicaltrials.gov identifiers: NCT00771901, NCT01877551) on insulin-resistant subjects (a population typically also affected by increased body adiposity), our results caution for evaluation of cancer risk in these patients.

It is important to note that we have studied the effects of relatively short-term HCD on KRAS-driven lung tumors. Thus, long-term outcomes and the contribution of obesity and/or other metabolic defects caused by HCD to tumor behavior remain to be evaluated. Also, while our pharmacological data shown in Figures 3A–3F and S3A–S3I suggest that unresolved ER stress underlies reduced tumor growth in HCD-pre-tumor-onset *Kras*^{G12D} mice, further genetic studies will be needed to fully dissect the underpinning mechanisms. Lastly, our data warrant thorough epidemiological assessment of lung cancer risk in obese people.

In summary, we unveiled an anti-tumor effect of HCD feeding on KRAS-driven lung tumorigenesis. Unresolved ER stress owing to impaired UPR^{ER} underlies, at least in part, the anti-tumor action of HCD. Hence, we propose that this vulnerability of KRAS-driven lung tumors could be targeted for therapeutic purposes. Importantly, we also identified FKBP10 as a putative anti-cancer target.

EXPERIMENTAL PROCEDURES

Mouse Generation and Studies

CCSP-rtTA/Tet-op-K-ras mice (FVB/SV129 mixed background) were generated as previously described (Konstantinidou et al., 2013) and housed in

groups of 4–5 with food (either SD or HCD; D12331 from Research Diets) and water available ad libitum in light- and temperature-controlled environments. Drinking water was supplemented with doxycycline at the concentration of 200 μg/ml. TUDCA was administered by intraperitoneal injection (250 mg/kg at 8 a.m. and 250 mg/kg at 8 p.m.). 4-PBA was administered at the same time points (500 mg/kg) by oral gavage. Care of mice at UTSW Medical Center at Dallas and at University of Geneva was within the procedures approved by Institutional Animal Care and Use Committee and by the animal care and experimentation authorities of the Canton of Geneva, respectively. Xenograft experiments were performed by subcutaneous inoculation of cells into 8-week-old male SCID mice.

Immunoblotting, Immunohistochemistry, and Quantitative Real-Time PCR

These procedures were performed as previously described (Konstantinidou et al., 2013). Clinical data were collected at Università Politecnica delle Marche from samples from patients who signed a waiver of authorization.

Expression Profiling

Gene expression profiles were obtained from microdissected lung tumors using MouseWG-6 v2.0 Expression BeadChips (Illumina).

shRNAs, Virus Production, and Transduction of Cell Lines

pLKO vectors (Open Biosystems) were used to produce recombinant lentiviruses using TransIT-293T Mirus reagent following manufacturer's instructions. Human cell lines A549, H596, H1650, ASPC, and MDA-MB231 were transduced as previously described (Konstantinidou et al., 2013).

Carbonylated Protein Determination

Levels of carbonylated proteins were determined by ELISA (Enzo Life Sciences) following manufacturer's instructions.

Pharmacokinetics Assessments

Analytical assay of plasma, lung, and tumor samples was performed using a QTRAP 4000 LC-MS/MS system.

Statistical Analysis

Two-tail unpaired Student's t test or one-way ANOVA (Tukey's post test) was used when comparing two groups or more than two groups, respectively. Error bars represent SEM.

ACCESSION NUMBERS

Data have been deposited in the NCBI Gene Expression Omnibus and are accessible through the accession number GSE56260.

SUPPLEMENTAL INFORMATION

Supplemental Information includes Supplemental Experimental Procedures and four figures and can be found with this article online at http://dx.doi.org/10.1016/j.cmet.2014.11.020.

AUTHOR CONTRIBUTIONS

G.R., G.K., P.P.S., and R.C. conceived the study and wrote the paper. G.R., G.K., N.V., T.B., L.M., M.G., N.S.W., M.L., and A.S. performed the experiments and analyzed and interpreted the data.

ACKNOWLEDGMENTS

We thank Ariane Widmer, Anne Charollais, Carolyn Heckenmeyer, and Laurent Vinet for technical support; Drs. Claes Wollheim and Pedro Herrera (UNIGE) for critical reading of the manuscript; and Dr. James Richardson (UTSW) for pathological examination of the lungs. This work was supported by CPRIT RP101496 (G.K.), ACS Award 13-068-01-TBG and Lung Cancer SPORE P50CA70907 (P.P.S.), by European Commission (Marie Curie CIG 320898 and ERC-Consolidator 614847), and by Swiss National Science Foundation (310030_146533/1) (R.C.). This work has also received the unrestricted support of the Louis-Jeantet Foundation (R.C.).

Received: October 2, 2014
Revised: October 23, 2014
Accepted: November 24, 2014
Published: December 18, 2014

REFERENCES

Banks, A.S., Davis, S.M., Bates, S.H., and Myers, M.G., Jr. (2000). Activation of downstream signals by the long form of the leptin receptor. J. Biol. Chem. *275*, 14563–14572.

Bianchini, F., Kaaks, R., and Vainio, H. (2002). Overweight, obesity, and cancer risk. Lancet Oncol. *3*, 565–574.

Calle, E.E., and Kaaks, R. (2004). Overweight, obesity and cancer: epidemiological evidence and proposed mechanisms. Nat. Rev. Cancer *4*, 579–591.

Calle, E.E., and Thun, M.J. (2004). Obesity and cancer. Oncogene *23*, 6365–6378.

Dahlberg, S.E., Schiller, J.H., Bonomi, P.B., Sandler, A.B., Brahmer, J.R., Ramalingam, S.S., and Johnson, D.H. (2013). Body mass index and its association with clinical outcomes for advanced non-small-cell lung cancer patients enrolled on Eastern Cooperative Oncology Group clinical trials. J. Thorac. Oncol. *8*, 1121–1127.

Engelman, J.A. (2009). Targeting PI3K signalling in cancer: opportunities, challenges and limitations. Nat. Rev. Cancer *9*, 550–562.

Fisher, G.H., Wellen, S.L., Klimstra, D., Lenczowski, J.M., Tichelaar, J.W., Lizak, M.J., Whitsett, J.A., Koretsky, A., and Varmus, H.E. (2001). Induction and apoptotic regression of lung adenocarcinomas by regulation of a K-Ras transgene in the presence and absence of tumor suppressor genes. Genes Dev. *15*, 3249–3262.

Guerra, C., Schuhmacher, A.J., Cañamero, M., Grippo, P.J., Verdaguer, L., Pérez-Gallego, L., Dubus, P., Sandgren, E.P., and Barbacid, M. (2007). Chronic pancreatitis is essential for induction of pancreatic ductal adenocarcinoma by K-Ras oncogenes in adult mice. Cancer Cell *11*, 291–302.

Kalaany, N.Y., and Sabatini, D.M. (2009). Tumours with PI3K activation are resistant to dietary restriction. Nature *458*, 725–731.

Khandekar, M.J., Cohen, P., and Spiegelman, B.M. (2011). Molecular mechanisms of cancer development in obesity. Nat. Rev. Cancer *11*, 886–895.

Konstantinidou, G., Ramadori, G., Torti, F., Kangasniemi, K., Ramirez, R.E., Cai, Y., Behrens, C., Dellinger, M.T., Brekken, R.A., Wistuba, I.I., et al. (2013). RHOA-FAK is a required signaling axis for the maintenance of KRAS-driven lung adenocarcinomas. Cancer Discov *3*, 444–457.

Lee, J., Sun, C., Zhou, Y., Lee, J., Gokalp, D., Herrema, H., Park, S.W., Davis, R.J., and Ozcan, U. (2011). p38 MAPK-mediated regulation of Xbp1s is crucial for glucose homeostasis. Nat. Med. *17*, 1251–1260.

Leung, C.C., Lam, T.H., Yew, W.W., Chan, W.M., Law, W.S., and Tam, C.M. (2011). Lower lung cancer mortality in obesity. Int. J. Epidemiol. *40*, 174–182.

Lietman, C.D., Rajagopal, A., Homan, E.P., Munivez, E., Jiang, M.M., Bertin, T.K., Chen, Y., Hicks, J., Weis, M., Eyre, D., et al. (2014). Connective tissue alterations in Fkbp10-/- mice. Hum. Mol. Genet. *23*, 4822–4831.

Lu, M., Lawrence, D.A., Marsters, S., Acosta-Alvear, D., Kimmig, P., Mendez, A.S., Paton, A.W., Paton, J.C., Walter, P., and Ashkenazi, A. (2014). Cell death. Opposing unfolded-protein-response signals converge on death receptor 5 to control apoptosis. Science *345*, 98–101.

Mouchiroud, L., Houtkooper, R.H., Moullan, N., Katsyuba, E., Ryu, D., Cantó, C., Mottis, A., Jo, Y.S., Viswanathan, M., Schoonjans, K., et al. (2013). The NAD(+)/Sirtuin Pathway Modulates Longevity through Activation of Mitochondrial UPR and FOXO Signaling. Cell *154*, 430–441.

Ozcan, U., Cao, Q., Yilmaz, E., Lee, A.H., Iwakoshi, N.N., Ozdelen, E., Tuncman, G., Görgün, C., Glimcher, L.H., and Hotamisligil, G.S. (2004). Endoplasmic reticulum stress links obesity, insulin action, and type 2 diabetes. Science *306*, 457–461.

Ozcan, U., Yilmaz, E., Ozcan, L., Furuhashi, M., Vaillancourt, E., Smith, R.O., Görgün, C.Z., and Hotamisligil, G.S. (2006). Chemical chaperones reduce ER stress and restore glucose homeostasis in a mouse model of type 2 diabetes. Science *313*, 1137–1140.

Pao, W., Wang, T.Y., Riely, G.J., Miller, V.A., Pan, Q., Ladanyi, M., Zakowski, M.F., Heelan, R.T., Kris, M.G., and Varmus, H.E. (2005). KRAS mutations and primary resistance of lung adenocarcinomas to gefitinib or erlotinib. PLoS Med. *2*, e17.

Park, E.J., Lee, J.H., Yu, G.Y., He, G., Ali, S.R., Holzer, R.G., Osterreicher, C.H., Takahashi, H., and Karin, M. (2010a). Dietary and genetic obesity promote liver inflammation and tumorigenesis by enhancing IL-6 and TNF expression. Cell *140*, 197–208.

Park, S.W., Zhou, Y., Lee, J., Lu, A., Sun, C., Chung, J., Ueki, K., and Ozcan, U. (2010b). The regulatory subunits of PI3K, p85alpha and p85beta, interact with XBP-1 and increase its nuclear translocation. Nat. Med. *16*, 429–437.

Park, S.W., Herrema, H., Salazar, M., Cakir, I., Cabi, S., Basibuyuk Sahin, F., Chiu, Y.H., Cantley, L.C., and Ozcan, U. (2014). BRD7 regulates XBP1s' activity and glucose homeostasis through its interaction with the regulatory subunits of PI3K. Cell Metab. *20*, 73–84.

Patterson, C.E., Schaub, T., Coleman, E.J., and Davis, E.C. (2000). Developmental regulation of FKBP65. An ER-localized extracellular matrix binding-protein. Mol. Biol. Cell *11*, 3925–3935.

Pellegrino, M.W., Nargund, A.M., and Haynes, C.M. (2013). Signaling the mitochondrial unfolded protein response. Biochim. Biophys. Acta *1833*, 410–416.

Pylayeva-Gupta, Y., Grabocka, E., and Bar-Sagi, D. (2011). RAS oncogenes: weaving a tumorigenic web. Nat. Rev. Cancer *11*, 761–774.

Ramadori, G., Fujikawa, T., Anderson, J., Berglund, E.D., Frazao, R., Michán, S., Vianna, C.R., Sinclair, D.A., Elias, C.F., and Coppari, R. (2011). SIRT1 deacetylase in SF1 neurons protects against metabolic imbalance. Cell Metab. *14*, 301–312.

Ranganathan, A.C., Ojha, S., Kourtidis, A., Conklin, D.S., and Aguirre-Ghiso, J.A. (2008). Dual function of pancreatic endoplasmic reticulum kinase in tumor cell growth arrest and survival. Cancer Res. *68*, 3260–3268.

Ron, D. (2002). Translational control in the endoplasmic reticulum stress response. J. Clin. Invest. *110*, 1383–1388.

Schubbert, S., Shannon, K., and Bollag, G. (2007). Hyperactive Ras in developmental disorders and cancer. Nat. Rev. Cancer *7*, 295–308.

Szegezdi, E., Logue, S.E., Gorman, A.M., and Samali, A. (2006). Mediators of endoplasmic reticulum stress-induced apoptosis. EMBO Rep. *7*, 880–885.

Taubes, G. (2012). Cancer research. Unraveling the obesity-cancer connection. Science *335*, 28–30–32.

Vansaun, M.N. (2013). Molecular pathways: adiponectin and leptin signaling in cancer. Clin. Cancer Res. *19*, 1926–1932.

Vianna, C.R., and Coppari, R. (2011). A treasure trove of hypothalamic neurocircuitries governing body weight homeostasis. Endocrinology *152*, 11–18.

Walter, P., and Ron, D. (2011). The unfolded protein response: from stress pathway to homeostatic regulation. Science *334*, 1081–1086.

Yang, Y., Dong, J., Sun, K., Zhao, L., Zhao, F., Wang, L., and Jiao, Y. (2013). Obesity and incidence of lung cancer: a meta-analysis. Int. J. Cancer *132*, 1162–1169.

Zoncu, R., Efeyan, A., and Sabatini, D.M. (2011). mTOR: from growth signal integration to cancer, diabetes and ageing. Nat. Rev. Mol. Cell Biol. *12*, 21–35.

Cell Metabolism, Volume *21*

Supplemental Information

Diet-Induced Unresolved ER Stress Hinders KRAS-Driven Lung Tumorigenesis

Giorgio Ramadori, Georgia Konstantinidou, Niranjan Venkateswaran, Tommasina Biscotti, Lorraine Morlock, Mirco Galié, Noelle S. Williams, Michele Luchetti, Alfredo Santinelli, Pier Paolo Scaglioni, and Roberto Coppari

Supplemental data

Supplemental Figures

Supplemental Figure 1

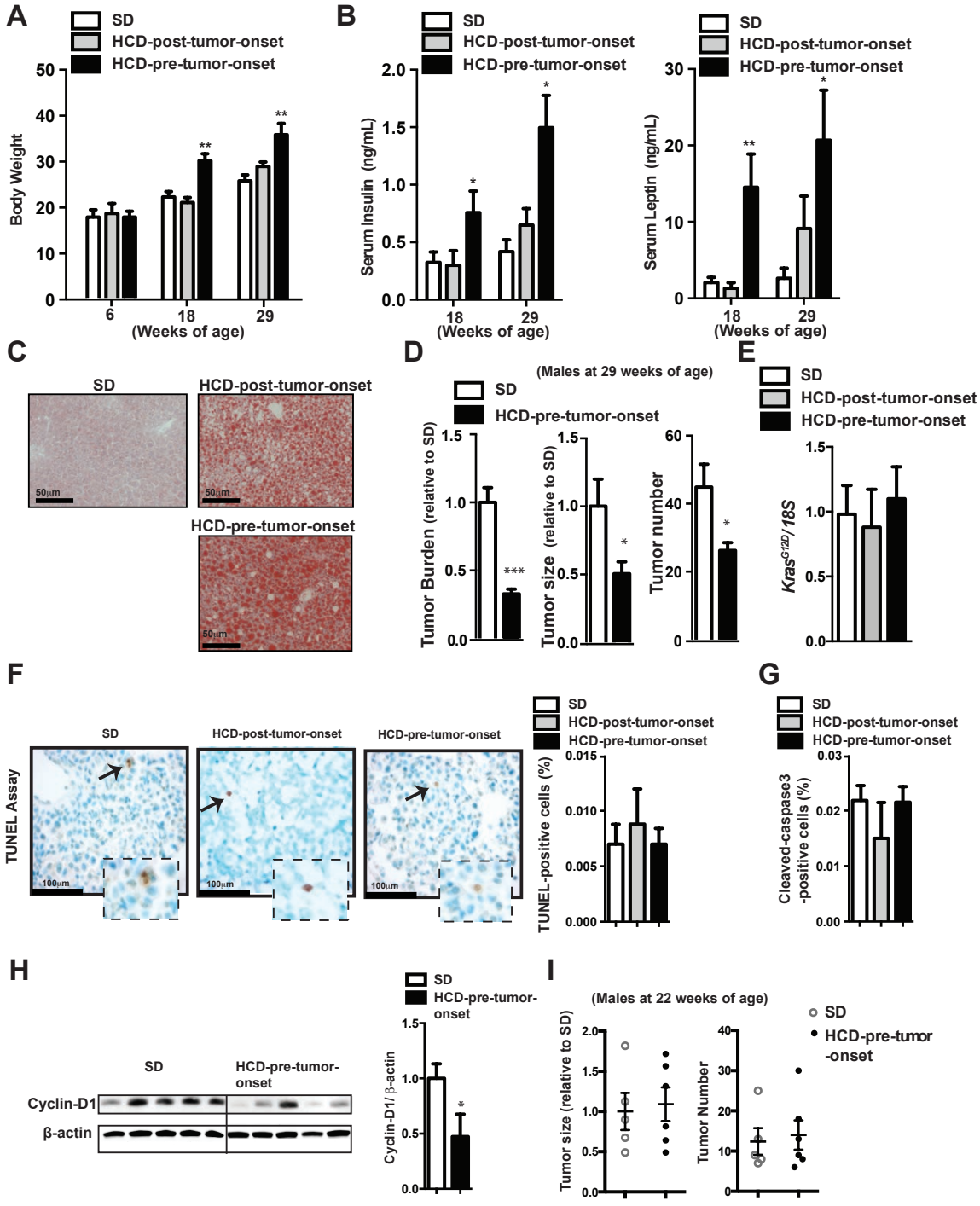

Supplemental Figure 1, related to Figure 1. Effect of chronic HCD feeding on KRAS-driven lung tumorigenesis. In **(A-H)** SD, HCD-post-tumor-onset and HCD-pre-tumor-onset *Kras*^{G12D} mice were treated as shown in Figure 1A. **(A)** Body weight, **(B)** serum leptin and insulin levels and **(C)** liver Oil-Red-O staining from age-matched 18- and 29-weeks-old SD, HCD-post-tumor-onset and HCD-pre-tumor-onset *Kras*^{G12D} mice (females; n=5-7 mice/ group). **(D)** Quantification of tumor burden, number and size in 29-week-old SD and HCD-pre-tumor-onset *Kras*^{G12D} mice (males; n=5-6/ group). **(E)** mRNA level of *Kras*^{G12D} in micro-dissected lung tumors and **(F)** representative images of lung tumor sections stained for TUNEL assay (in brown TUNEL positive cells) and relative quantification histograms of 29 weeks-old SD, HCD-post-tumor-onset and HCD-pre-tumor-onset *Kras*^{G12D} mice (females; n=5-7 mice/ group), **(G)** quantification of cleaved-caspase-3 positive cells and **(H)** immunoblots from total cell lysates of micro-dissected tumors of 29 weeks-old SD- and HCD-pre-tumor-onset *Kras*^{G12D} mice (males; n=5 mice for group). **(I)** Quantification of tumor burden and tumor number in 22 weeks-old SD- and HCD-pre-tumor-onset *Kras*^{G12D} mice (males; n=5 mice for group). Error bars represent s.e.m. Statistical analyses were done using one-way ANOVA (Tukey's post test). *P<0.05, **P<0.01, ***P<0.001.

Supplemental Figure 2 (part A)

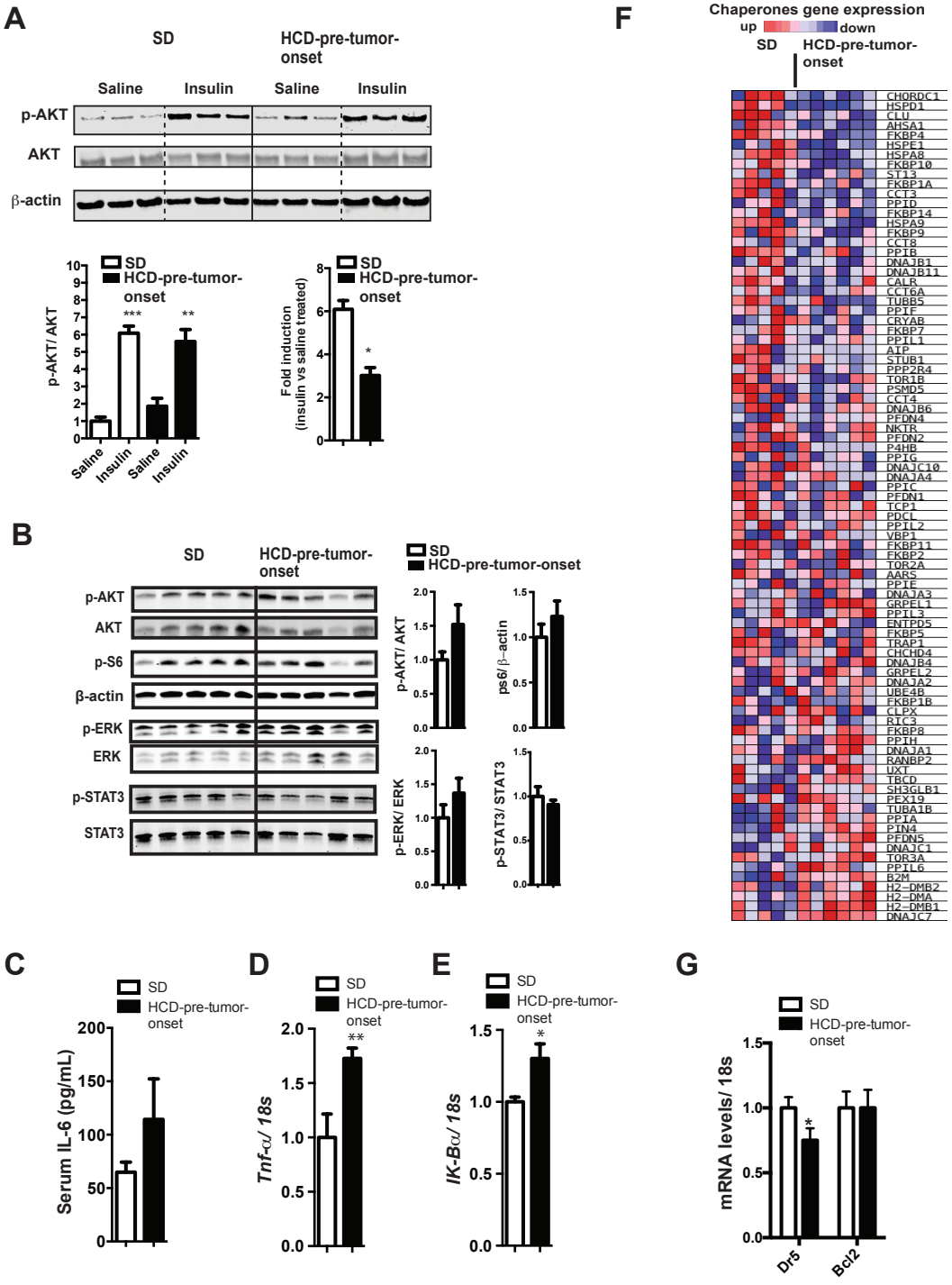

Supplemental Figure 2 (part B)

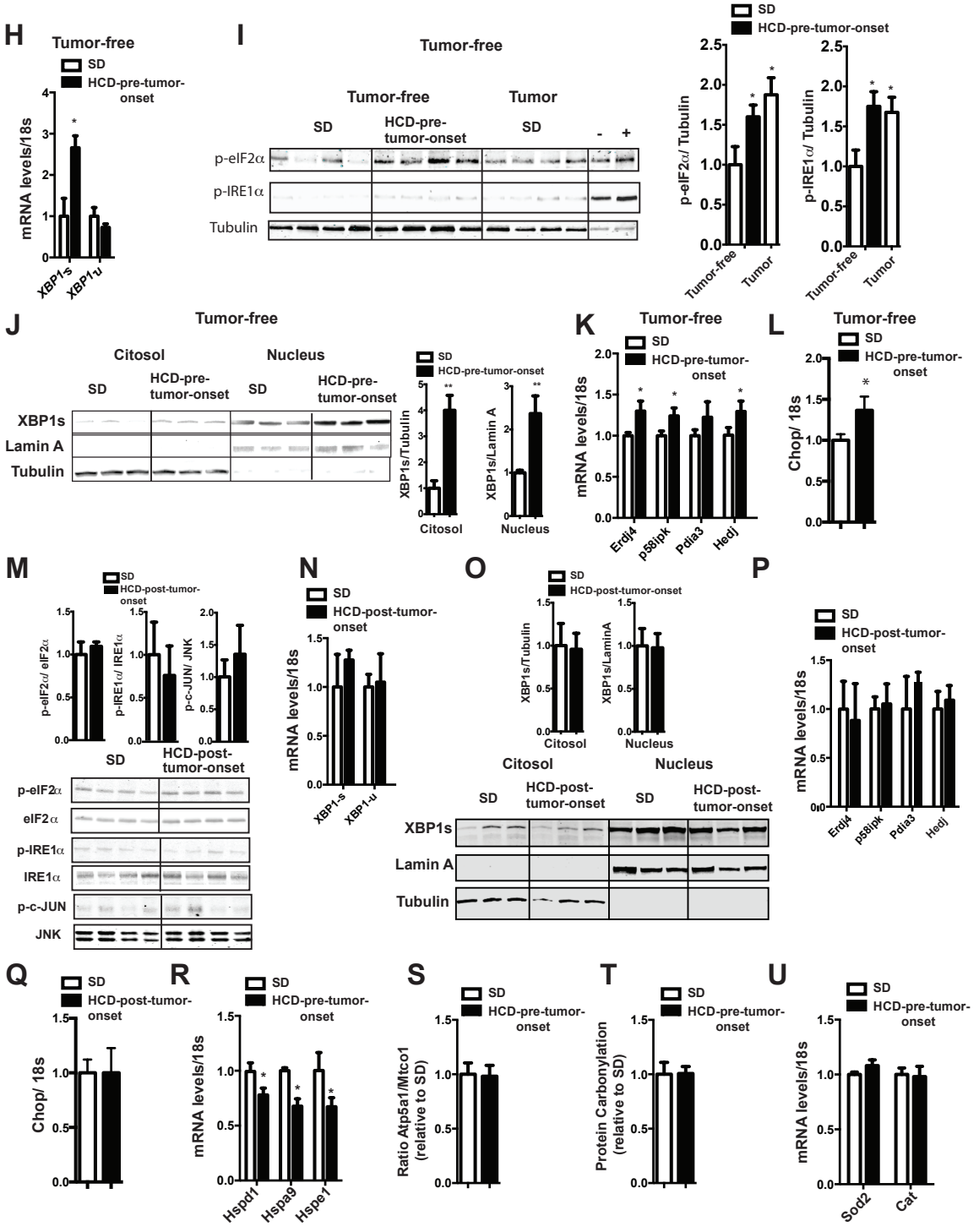

Supplemental Figure 2, related to Figure 2. Unresolved ER-stress in lung tumors of HCD-pre-tumor-onset *Kras^{G12D}* mice. **(A)** Immunoblot and quantification of pAKT relative to total AKT in micro-dissected lung tumors of 29-week-old HCD-pre-tumor-

onset or SD-mice after 10' of treatment with 15U/kg of insulin or saline (n=3/group). **(B)** Immunoblots from total cell lysates of micro-dissected lung tumors (values normalized to total protein levels or β-actin levels), **(C)** Serum IL-6 levels, **(D-E)** mRNA levels in micro-dissected tumors of 29-week-old HCD-pre-tumor-onset and SD mice. **(F)** Heat maps of the genes encoding for chaperones enriched in a genome-wide expression profiling illustrating the changes in gene expression between micro-dissected tumors of 29-week-old HCD-pre-tumor-onset and SD mice (expression levels shown are representative of each replicate from micro-dissected lung tumors). Red signal denotes higher expression relative to the mean expression level within the group and blue signal denotes lower expression relative to the mean expression level within the group. **(G)** mRNA levels in micro-dissected tumors of 29-week-old HCD-pre-tumor-onset and SD mice. **(H)** mRNA levels, **(I)** immunoblots from whole lysate and relative quantification, **(J)** immunoblots from cytosolic and nuclear fraction of lysates and relative quantification, **(K and L)** mRNA levels, from tumor-free lung tissue of 29-week-old HCD-pre-tumor-onset and SD mice. **(M and O)** Immunoblots and relative quantification and **(N,P and Q)** mRNA levels from lysate of micro-dissected tumors of 29-week-old HCD-post-tumor-onset and SD mice. **(R and U)** mRNA levels, **(S)** mRNA ratio, and (**T**) protein carbonylation in micro-dissected tumors of 29-week-old HCD-pre-tumor-onset and SD mice. In **(B-U)** mice were treated as shown in Figure 1A (males; n=5-6/ group). Error bars represent s.e.m. Statistical analyses were done using two-tailed unpaired Student's t test or using one-way ANOVA (Tukey's post test). *P<0.05, **P<0.01.

Supplemental Figure 3

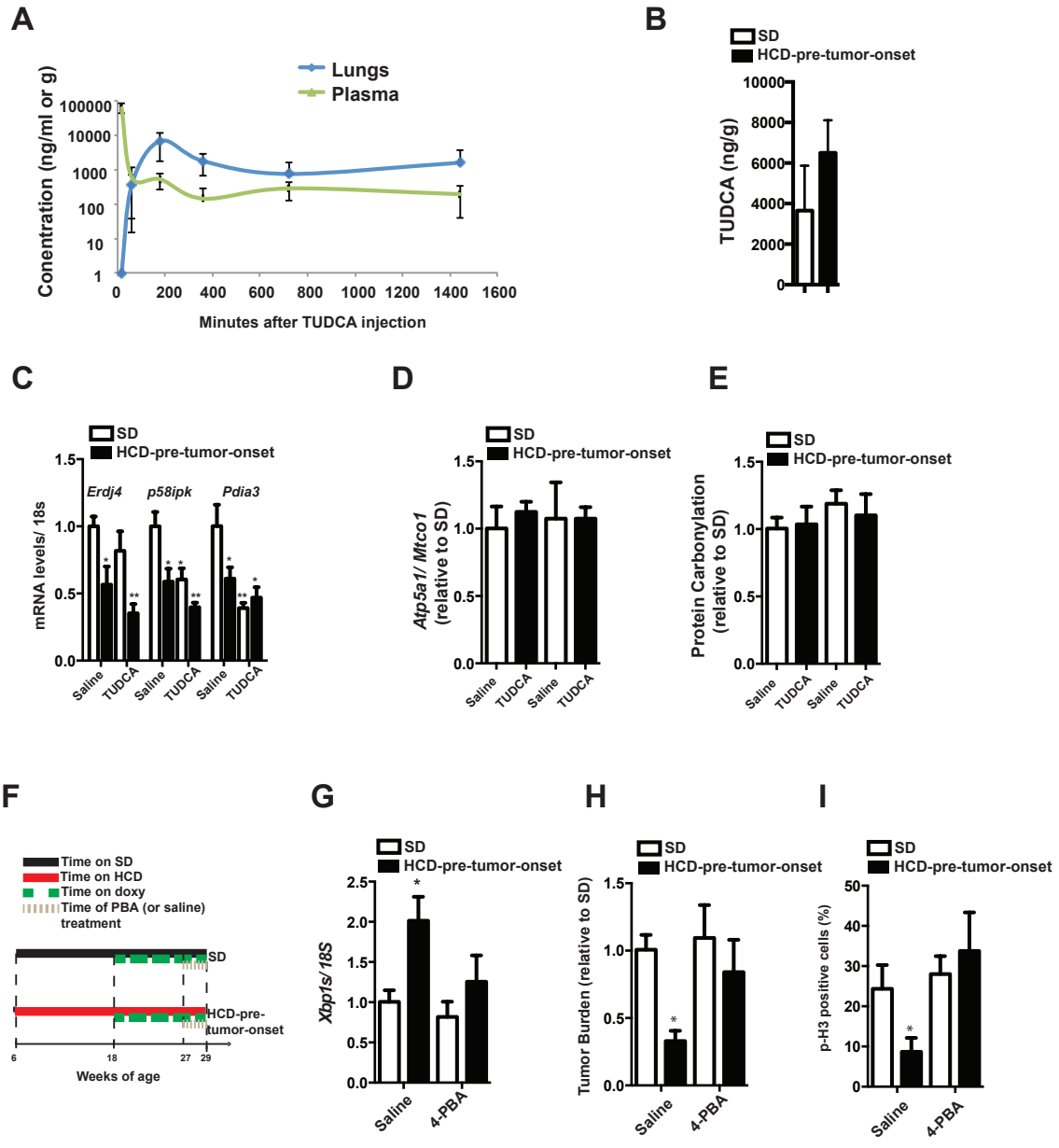

Supplemental Figure 3, related to Figure 3. Treatment with chemical chaperones reverses the anti-tumor effect of HCD feeding on KRAS-driven lung tumors. (A) TUDCA pharmacokinetics in plasma and lung of mice after a single intraperitoneal injection of TUDCA (dose= 250mg/kg). **(B)** TUDCA accumulation in dissected tumors of HCD-pre-tumor-onset and SD mice after 3 hours after the last injection of 5 days of

treatment. (C) mRNA levels, **(D)** mRNA ratio and **(E)** protein carbonylation, from microdissected tumor of HCD-pre-tumor-onset and SD mice treated with TUDCA or saline. **(F)** Time table of mouse treatments, **(G)** mRNA levels, **(H)** tumor burden and **(I)** tumor proliferation in HCD-pre-tumor-onset and SD mice treated as shown in **(F)** (males; n=4-5/ group). Error bars represent s.e.m. Statistical analyses were done using one-way ANOVA (Tukey's post test). *P<0.05, **P<0.01.

Supplemental Figure 4

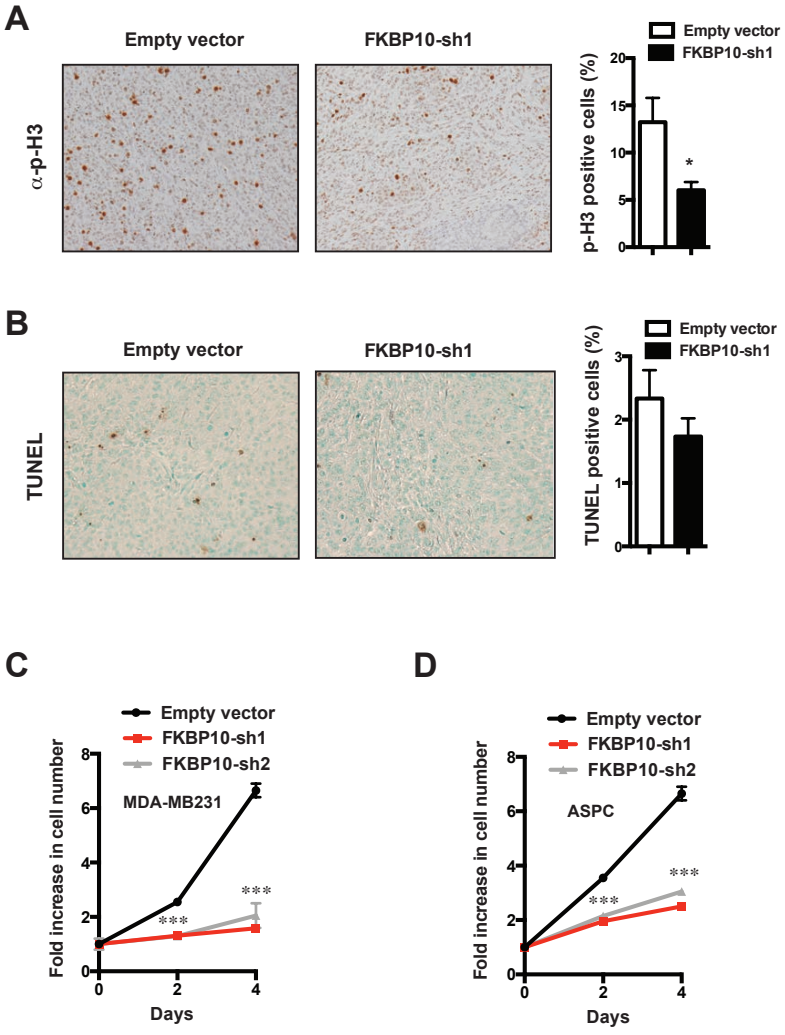

Supplemental Figure 4, related to Figure 4. Unraveling FKBP10 as a novel therapeutic target for KRAS-driven lung cancer. **(A)** Representative images of tumor sections stained with anti-p-H3 (p-H3 positive cells in dark-brown) and histograms indicating % of p-H3 positive cells/tumor cells (n=5 for group). **(B)** Representative images of tumor sections stained for TUNEL assay (in brown TUNEL positive cells) and relative quantification histograms indicating % of TUNEL positive cells/tumor cells (n=5 for group). **(C)** Anti-proliferative effect of FKBP10 knockdown in MDA-MB231 (cell line from human mammary adenocarcinoma) and **(D)** ASPC (cell line from human pancreatic ductal adenocarcinoma) cells. Error bars represent s.e.m. Statistical analyses were done using two-tailed unpaired Student's t test or using one-way ANOVA (Tukey's post test). *P<0.05, ***P<0.001.

Supplemental Methods.

Mouse generation and studies

CCSP-rtTA/Tet-op-K-ras mice (FVB/SV129 mixed background) were generated as previously described (Konstantinidou et al., 2009; Konstantinidou et al., 2013). Mice were housed in groups of 4-5 with food (either a standard chow rodent diet or the high-calorie (HC) diet (D12331 from Research Diets, New Brunswick, NJ, USA) and water available *ad libitum* in light- and temperature-controlled environments. Drinking water has been supplemented with doxycycline at the concentration of 200 μg/mL for the length of time indicated in the figure legends. TUDCA (Calbiochem) resuspended in saline at the concentration of 100 mg/mL (or saline for the controls) was administered by

intraperitoneal injection (250mg/kg at 8am and 250mg/kg at 8pm). 4-PBA (Calbiochem) was administered at the same time points (500 mg/kg for 8am and 8pm, total 1g/kg/day) by oral gavage. Controls for PBA, received the same volume of vehicle by gavage of the PBA-treated mice. Tumor burden was assessed by digital quantification of the area occupied by tumors in the left lobe compared to unaffected tissue using NIH ImageJ (v1.42q) software. Tumor number was assessed by microscope analysis of lung sections stained with H&E and defined as the average of the number of adenomas present in three adjacent sections of the left lobe. Tumor size is defined as the ratio between tumor area arbitrary values (using NIH ImageJ (v1.42q) software) and tumor number in the left lobe. Fed hormones/metabolites levels were determined by collecting tail blood from mice that were without food for 3 hours. Fasted hormones/metabolites levels were assessed in mice provided only with water *ad libitum* and without food for the indicated period. Time of day at which blood was collected was the same between groups. Tail vein blood was assayed for glucose levels using a standard glucometer (Fisher Scientific, Morris Plains, NJ). Serum was collected by centrifugation and assayed for leptin (Crystal Chem. Inc., Downers Grove, IL) and insulin (Crystal Chem. Inc.) levels using commercially available kits. Xenograft experiments were performed by subcutaneous inoculation of 10^6 cells into 8-week-old male SCID mice. Tumor volumes were calculated every three days using the formula: (length X width^2) /2.

Immunoblotting

Immunoblots were performed according to standard procedures in RIPA buffer (150 mM NaCl, 10 mM Tris pH 7.5, 1% NP40, 1% Deoxycholate, 0.1% SDS) and supplemented

with phosphatase and protease inhibitors (SIGMA). Samples were resolved on EZ-Run™ 10% Protein Gel Solution (Fisher Scientific), blotted on Protran® membrane 0.2 μm (Whatman) and developed with Li-Cor imaging System. The following antibodies were used: p-AKT^{Ser473}, total AKT, p-ERK1/2$^{Thr202/Tyr204}$, total ERK1/2, p-eIF2α, eIF2α, p-STAT3, STAT3, p-S6, p-c-Jun, Cyclin D1 and P58IPK (Cell Signaling); β–Actin (Sigma); XBP1-s, p-IRE1α, IRE1a and Lamin A and Tubulin (Abcam); total JNK (Santa Cruz); PDIA3 (GeneTex Antibodies); FKBP10 (ProteinTech).

Immunohistochemistry

Mouse lungs and tumors were fixed in 4% paraformaldehyde (PFA) overnight at 4°C. IHC procedure was performed as previously described (Konstantinidou et al., 2009; Konstantinidou et al., 2013), using a commercial antibody against p-H3 (Millipore) and cleaved-caspase-3 (Cell Signaling). To detect apoptosis in mouse lung tissue we used the ApopTag plus peroxidase in situ apoptosis detection kit (Millipore). Methyl-green was used as counterstaining in TUNEL assay. Hematoxylin was used as conterstaining in IHC for p-H3 and cleaved-caspase-3. In order to quantify the % of p-H3 and TUNEL-positive cells, a total of 200 cells were scored/slide for at least 3 replicates.

In order to determine FKBP10 expression in human paraffin embedded lung samples we used the following procedure. Sections of 3-5 μm thick were deparaffinized and the detection of antigens has occurred in automated manner with DAKO PT Link using ENVISION™ FLEX TARGET RETRIEVAL SOLUTION LOW pH (50X) (DAKO) at a temperature of 98°C. After 70 minutes of treatment, sections were treated with 3% hydrogen peroxide and incubated for 30 minutes with unconjugated anti-mouse IgG at

RT. Subsequently sections were incubated for 1 hour at RT with mouse Anti-FKBP65 antibody (1:750, BD Transduction Laboratories™). The staining was completed using ENVISION FLEX ™/HRP (DAKO), as detection system; 3,3- diaminobenzidine-hydrogen peroxide was used as chromogen. Then, the slides were counterstained with Meyer's hematoxylin for 1 minute, dehydrated in a graded series of alcohol, treated with xylene, and coverslipped. Immunohistochemical staining was semi-quantitatively assessed by considering the "percentage of positive tumor cells" (range 0-100%).

Quantitative real-time PCR

RNA was extracted using a RNA extraction kit (Qiagen). Complementary DNA was generated by Superscript II (Invitrogen) and used with SYBR Green PCR master mix (Applied Biosystem) for quantitative real time PCR (q-RTPCR) analysis. mRNA contents were normalized to *18-S*. Sequences of deoxy-oligonucleotides primers used are outlined here: *Erdj4* 5'CCCCAGTGTCAAACTGTACCAG and 5'AGCGTTTCCAATTTTCCATAAATT; *p58ipk* 5'CAGTTGATGGTGACCCCGAT and 5'GTCTTGCGGCAGTAAAGTCC; *Pdia3* 5' TGTTGGAACTGACGGACGAA and 5'GGCGAAGAACTCGACTAGCA; *Hedj* 5'AGGAGCGAAGAGAACTGGACT and 5'AAATGACTCCAATCCCCAGCC; *Xbp1-s* 5'CTGAGTCCGCAGCAGGT and 5'TGTCAGAGTCCATGGGAAGA; *Xbp1-u* 5'CTGAGTCCGCAGCACTCAGA and 5' TCAGAGTCCATGGGAAGATGTTC; *Chop* 5'ACCTGAGGAGAGAGTGTTCCA and 5'CAAGGTGAAAGGCAGGGACT; *18S* 5'ACCGCAGCTAGGAATAATGGA and 5'GCCTCAGTTCCGAAAACCA; *Dr5* 5'GGAGCTCTGCTTGTCTGGAA and 5'CGTGCTAGATGTCTGTCGGT; *Bcl2* 5'TTCTTTGAGTTCGGTGGGGTC and

5'TGGGGCCATATAGTTCCACAA; *Hspd1* 5'TCAGTCCATTGTCCCTGCTC and 5'AACCAGCGTGCTTAGAGCTT; *Hspa9* 5'CAAGGGTGCAGTGGTTGGTA and 5'GGGGTAGTTCTGGCACCTTC; *Hspe1* 5'TGAAAGGAGTGCTGCCGAAA and 5'TTCCTTTCCCTCCTGACCCC; *Sod2* 5'GCCTCCCAGACCTGCCTTAC and 5'GTGGTACTTCTCCTCGGTGGCG; *Cat* 5'AGGACCGTGTTTGGTTGCTT and 5'CCGCTGGCGCTTTTATTGT. All assays were performed using an Applied Biosystems Prism 7900HT sequence detection system. For each mRNA assessment, quantitative RT-PCR analyses were repeated at least 3 times.

Expression profiling

Gene expression profiles were obtained from micro-dissected lung tumors of 29-week old mice. For total RNA extraction we used a RNA isolation kit (Qiagen) followed by DNase digestion and cleanup according to the manufacturer's instructions. Microarray was performed by UTSW Microarray Core facility (http://microarray.swmed.edu) using Illumina MouseWG-6 v2.0 Expression BeadChips (Illumina, NC, USA). The Selected enriched groups of genes where analyzed by Gene Set Enrichment Analysis (GSEA) (Huang da et al., 2009). The data have been deposited in NCBI's Gene Expression Omnibus and are accessible through GEO Series accession number GSE56260.

shRNAs, virus production and transduction

The pLKO lentiviral vectors encoding shRNAs targeting *FKBP10* were purchased from Open Biosystems. Clones IDs were the following: 1) TCRN0000053928, 2) TCRN0000053929, 3) TCRN0000053930, 4) TCRN0000053931, 5) TCRN0000053932.

We produced recombinant lentiviruses by transfecting 293T cells, using TransIT-293 tranfection reagent (Mirus), with pMD2G (VSV-G protein), pCMV-dR8.74 (lentivirus packaging vector) and lentiviral constructs.

Cell lines

Human cell lines A549, H596, H1650, ASPC and MDA-MB231 were from the Hamon Center cell line repository (UT Southwestern Medical Center). All cell lines were DNA-fingerprinted for provenance (PowerPlex 1.2 Kit; Promega) and Mycoplasma-free (e-Myco Kit; Boca Scientific).

Carbonylated protein determination.

Levels of carbonylated proteins in lysates from tumors were determined by ELISA (Enzo Life Sciences) following manufacturers' instructions.

Pharmacokinetics assessments.

Analytical processing of plasma samples: 100µl of plasma were mixed with 200µl of methanol containing 0.15% formic acid and 37.5 ng/ml n-benzylbenzamide internal standard (IS). The samples were vortexed 15 sec, incubated at room temp for 10 min and spun twice at 16,100 x g 5 min 4ºC in a standard microcentrifuge. TUDCA levels were then monitored by LC-MS/MS using an AB/Sciex (Applied Biosystems, Foster City, CA) 4000 Qtrap mass spectrometer coupled to a Shimadzu (Columbia, MD) Prominence LC. The compound was detected using electrospray ionization with the mass spectrometer in

positive MRM (multiple reaction monitoring) mode by following the precursor to fragment ion transition 522.4 (M + Na+) → 486.4.

Analytical processing of lung and tumor samples: samples from lungs or tumors were prepared by homogenizing tissue in a three (Fig S3A) or six (Fig S3B)- fold volume of PBS100 µl of homogenized tissue solution were mixed with 25 µl of 12.5% perchloric acid (PCA). The samples were vortexed 15 sec and centrifuged at 16,100 x g for 5min at 4ºC in standard microcentrifuge tubes. Aliquots of 75 µl were neutralized with 75 µl of 350 mM KOH and 75 µl of 175 mM KHCO3. These samples were vortexed 15 sec and centrifuged again at 16,100 x g for 5 min at 4ºC in standard microcentrifuge tubes. Aliquots of 180µl of supernatant were put into HPLC vials with inserts and spiked with 0.9 µl of 1 ng/µl n-benzylbenzamide IS vortexed and analyzed by QTRAP 4000 LC-MS/MS system as described for plasma.

Supplemental References

Huang da, W., Sherman, B.T., and Lempicki, R.A. (2009). Systematic and integrative analysis of large gene lists using DAVID bioinformatics resources. Nat Protoc *4*, 44-57.

Konstantinidou, G., Bey, E.A., Rabellino, A., Schuster, K., Maira, M.S., Gazdar, A.F., Amici, A., Boothman, D.A., and Scaglioni, P.P. (2009). Dual phosphoinositide 3-kinase/mammalian target of rapamycin blockade is an effective radiosensitizing strategy for the treatment of non-small cell lung cancer harboring K-RAS mutations. Cancer Res *69*, 7644-7652.

Konstantinidou, G., Ramadori, G., Torti, F., Kangasniemi, K., Ramirez, R.E., Cai, Y., Behrens, C., Dellinger, M.T., Brekken, R.A., Wistuba, II, *et al.* (2013). RHOA-FAK is a required signaling axis for the maintenance of KRAS-driven lung adenocarcinomas. Cancer discovery *3*, 444-457.